Scientific Research Publishing

Materials Sciences and Applications, 2024, 15, 538-557
https://www.scirp.org/journal/msa
ISSN Online: 2153-1188
ISSN Print: 2153-117X

Study of the Influence of Clay in the Degradation of Methylene Blue by Photo-Fenton Process

Namory Méité[1*], Lébé Prisca Marie-Sandrine Kouakou[1], Alfred Niamien Kouamé[1], Aliou Guillaume Lemeyonouin Pohan[2], Issiaka Sanou[3], Gaoussou Cissé[4], Christelle Adja Kouakou[1], Yao Jonas Andji-Yapi[1]

[1]Laboratoire de Constitution et Réaction de la Matière (LCRM), UFR-Science des Structures de la Matière et Technologie (SSMT), Université Félix Houphouët-Boigny (UFHB), Abidjan, Côte d'Ivoire
[2]Departement de Mathématiques, Physique et Chimie, UFR des Sciences Biologiques, Université Pelefero Gon Coulibaly, Korhogo, Côte d'Ivoire
[3]Unité de Formation et de Recherche en Sciences Exactes et Appliquées (UFR/SEA), Laboratoire de Chimie et Energies Renouvelables (LaCER), Université Nazi BONI, Bobo-Dioulasso, Burkina Faso
[4]Institut National Polytechnique Houphouët Boigny (INP-HB) de Yamoussoukro, Yamoussoukro, Côte d'Ivoire
Email: *meite.namory53@ufhb.edu.ci

How to cite this paper: Méité, N., Kouakou, L.P.M.-S., Kouamé, A.N., Pohan, A.G.L., Sanou, I., Cissé, G., Kouakou, C.A. and Andji-Yapi, Y.J. (2024) Study of the Influence of Clay in the Degradation of Methylene Blue by Photo-Fenton Process. *Materials Sciences and Applications*, **15**, 538-557.
https://doi.org/10.4236/msa.2024.1511036

Received: June 22, 2024
Accepted: November 24, 2024
Published: November 27, 2024

Abstract

Industrial effluents from textile, tannery or printing activities often have a significant pollutant load composed of dyes that are difficult to biodegrade. These dyes pose a threat to the environment. To overcome this problem, various processes have been developed to eliminate these dyes in wastewater before their release into nature. Conventional biological or physical processes most often prove to be ineffective and expensive. It is therefore necessary to resort to other processes such as advanced oxidation processes (POA). This work therefore focuses on the study of the influence of clay in the degradation of Methylene Blue by the photo-Fenton process which is one of the advanced oxidation processes (POA), with the source of irradiation, natural light. To do this, two clays from Côte d'Ivoire referenced AB and Aga were the subject of a physicochemical and mineralogical characterization. The results showed that Aga clay is composed of 75.43% quartz, 12.72% kaolinite, 8.75% illite and 3.12% goethite and AB clay consists of 61, 36% kaolinite, 28.6% quartz and 10.10% illite. Under natural light irradiation the optimal amounts of Fenton reagents (iron: 10 mg; H_2O_2: 0.1 mL) were determined. Finally, the addition of clay to the photo-Fenton process made it possible to improve the degradation of the pollutant (Methylene Blue). Indeed, the yield increased from 92% for the photo-Fenton process to 98.43% with the addition of AB clay and 98.13% for the addition of Aga clay. The results of the degradation kinetics clearly

show that the degradation follows the pseudo-second order kinetics with correlation coefficients greater than 0.99.

Keywords

Methylene Blue, Clay, Photo-Fenton, Pollutant, Degradation

1. Introduction

The expansion of the industrial sector has been accompanied by a phenomenon of water pollution due to the accumulation of pollutants in wastewater from industries such as textiles, paper, cosmetics, rubber and plastics. These pollutants include Methylene Blue (MB), a basic dye, which is most commonly used in the dyeing of cotton, wood, silk and paper [1]. It provides vivid colors, has excellent color fastness and is easy to apply. Unfortunately, most dyes are persistent in receiving environments and have harmful effects on the environment and human health. Their elimination of wastewater is therefore essential. To this end, several physical, chemical and biological processes have been developed to eliminate or destroy these pollutants from industrial effluents. Among these processes, we can cite coagulation-flocculation, adsorption, membrane separation, etc. [2]. However, some of these methods have revealed limits linked, on the one hand, to the production of toxic by-products and, on the other hand, to the financial cost of implementation. These limitations make these methods inaccessible [3] [4]. Thus, advanced oxidation processes appear as alternative processes for the treatment of wastewater. Their aim is to achieve almost total mineralization of water loaded with pollutants. As part of our study, the choice fell on the photo-Fenton process. The two reagents in this process, hydrogen peroxide and iron salt, are available, inexpensive and pose no danger to the environment. This process will be associated with natural resources such as clay and natural light. Due to its adsorbent power, clay traps dyes. In fact, clay is a natural material with absorbent properties, it is inexpensive and widespread over most of the Ivorian territory. It has a set of very small particles having less than 2 μm in apparent diameter, which in contact with water slide over each other to account for the phenomenon of plasticity. Natural light available throughout the year with variable intensities can constitute an alternative source that is usable especially in developing countries. Indeed, this source of renewable energy is free and inexhaustible, it is by far the most abundant energy on earth. With the aim of valorizing clays, this work aims to study the elimination of Methylene Blue by the photo-Fenton process associated with clay.

2. Raw Materials and Experimental Techniques

2.1. Clay Raw Materials

Two clay raw materials are used in this study, "Aga" clay was taken from the town of Gagnoa located in the Center-West of Côte d'Ivoire, the sampling site

coordinates of 6˚07'37.6'N, 5˚56'15.0'W. The second sample noted "AB" comes from the Akouai-Agban deposit, in the suburbs of the town of Bingerville on the lagoon shore in the south of Côte d'Ivoire, the coordinates of the sampling site are 5˚16'12, 883844N, 3˚53'23.325'W. These samples are presented in Figure 1.

Figure 1. Images of Aga and AB clays.

2.2. Methods

2.2.1. Preparation of the Methylene Blue (MB) Solution

The solution to be treated (from BM) was prepared by introducing 0.0125 g of Methylene Blue powder into a 250 mL volumetric flask containing distilled water which was made up to the mark (*i.e.*, a solution concentration 0.05 g/L). The mixture obtained was homogenized by stirring using a magnetic bar for thirty minutes (30 min).

2.2.2. Experimental Approach for the Photo-Fenton Process

During this process, the MB solution is subjected to a treatment of hydrogen peroxide (H_2O_2) and ferrous iron (Fe^{2+}) in the presence of light in order to find the optimal concentrations of H_2O_2 and ferrous iron Fe^{2+}. The whole is placed on a magnetic stirrer at a moderate speed allowing its permanent homogenization via a magnetic bar immersed in it. A manual sample of 2 mL to be taken every 15 minutes for 2 hours using 5 mL syringes. The samples are analyzed using a UV-Visible spectrophotometer. During this approach, to study the influence of clay on the degradation of Methylene Blue by the photo-Fenton process, the optimal concentrations of hydrogen peroxide (H_2O_2) and ferrous iron are added to the BM solution. (Fe^{2+}) previously determined by the photo-Fenton process. In the entire mixture, we vary a quantity of clay from 0.05 g to 0.2 g. Everything is placed on a magnetic stirrer at a moderate speed allowing its permanent homogenization via a magnetic bar immersed in it. The sampling and analysis of the homogenized solution follow the approach described above.

2.3. Experimental Techniques

2.3.1. Determination of pH at the Point of Zero Charge

The isoelectric point or pH at the point of zero charge is the parameter which

corresponds to the pH for which the surface of the solid presents a zero charge [5]. To determine the pH at the point of zero charge of the clays used in this work, the method of Lopez-Ramon *et al.* taken from the thesis of N'guessan was used [6] [7]. Solutions of 0.1 mol·L^{-1} of NaCl and pH between 2 and 10 (adjusted by adding an aqueous solution of NaOH or H_2SO_4) were first prepared. The HI 2211 pH meter was used for pH measurement. 0.1 g of the different dried clays is brought into contact with 20 mL of each of the solutions contained in beakers. The solutions are stirred for 3 days at room temperature. Each solution is then filtered using filter paper (Double Rings Filter Paper) and a new pH measurement is carried out. We draw the curve C representing the final pH as a function of the initial pH. The pH_{PZC} then corresponds to the pH of the solution for which the curve C crosses the first bisector (final pH = initial pH).

2.3.2. Chemical Analysis

The aim of this technique is to determine the chemical composition of the clay sample using the ICP-AES (Industively Coupled Plasma-Atomic Emission Spectromely) Plasma Emission Spectrometer [8]. The sample to be characterized was put into solution and converted into an aerosol, then vaporized, atomized, excited and/or ionized. To do this, 30 mg of each sample is dried at 110˚C for 24 hours in a Teflon tube and the whole is introduced into a microwave device (CEM, MARCH 5).

2.3.3. X-Ray Diffraction

X-ray diffraction is an analysis method that makes it possible to identify the main crystallized mineral phases present in the material. The X-ray diffraction patterns are obtained using a Bruker D8 Advance type device equipped with a copper anticathode (λ = 1.54 Å).

2.3.4. Infrared Spectroscopy

Infrared spectroscopy is a technique for studying the nature and local environment of chemical bonds. It allows the determination of the functional group present in the material. There are three distinguished areas (near infrared, mid infrared and far infrared). For our study, the IR spectra was carried out in the mid-infrared domain using two spectrometers (Fourier Transform spectrometer (Tensor 27 Golden Gate Single) and Elmer Spectrum 1000 Fourier Transform spectrometer.

2.3.5. UV-Visible Spectrophotometry

Spectrophotometry is a quantitative analytical technique, which consists of measuring the absorbance or optical density of a given chemical substance in solution. The rate of decrease in light intensity as a function of the thickness of the absorbing medium is given by the Beer-Lambert law according to the equation (Equation (1)):

$$A = \log \frac{I_0}{I} = \varepsilon \cdot l \cdot C \quad (1)$$

With:

I_0: initial intensity of the light passed through; I: intensity of transmitted light; A: absorbance; C: concentration of absorbent species (mol·L^{-1}); l: optical path length in the solution (cm); ε: molecular absorption coefficient (L·mol^{-1}·cm^{-1}).

➢ **Determination of the calibration curve**

The aqueous BM solution was prepared by dissolving powdered BM in distilled water. The maximum absorption wavelength (λ_{max}) was obtained by scanning the λ between 200 and 800 nm. The peak of our dye is obtained at 663.1 nm. In order to obtain the MB calibration curve we prepared a stock solution with a concentration of 50 mg·L^{-1}. From the stock solution we determined the concentrations (1, 2, 3, 4, 5 mg·L^{-1}). These will subsequently be analyzed by UV-visible spectrophotometry. Figure 2 shows the BM calibration curve. The curve is linear over the interval of chosen concentrations, therefore the Beer-Lambert law is verified for this concentration range.

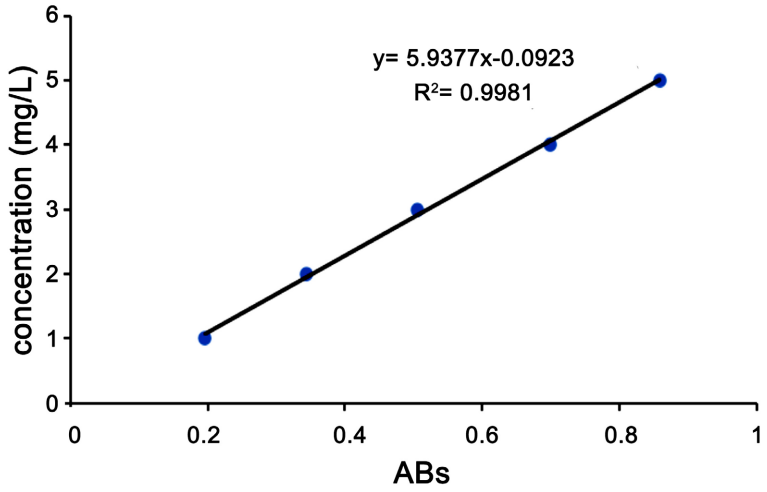

Figure 2. Calibration curve obtained for the determination of Methylene Blue by UV/Visible.

➢ **Determination of elimination rate**

The percentage of dye degradation was calculated using the equation (Equation (2)):

$$q_e = \frac{V}{m} \times \left(C_0 - C_e\right) \tag{2}$$

$$E(\%) = \frac{C_0 - C_e}{C_0} \times 100 \tag{3}$$

q_e: the quantity adsorbed per unit of clay (mg·g^{-1}); V: volume of MB solution (mL); m: the mass of the clay (g); C_0: the initial concentration of BM (mg·L^{-1}); C_e: the equilibrium concentration of BM (mg·L^{-1}); E: MB elimination rate (%).

2.3.6. Study of Degradation Kinetics

Several kinetic models have been used to interpret the experimental data [9]. The

two commonly used kinetics models are: the pseudo-first-order model (PPO), the pseudo-second-order model (PSO).

1) Pseudo-first order model

Lagergren proposed a pseudo-first order kinetic model expressed by the following relation [9] (Equation (4)):

$$\frac{\mathrm{d}q_t}{\mathrm{d}t} = k_1\left(q_e - q_t\right) \tag{4}$$

with k_1 the rate constant for pseudo first order kinetics (min^{-1}), t the contact time (min), q_t and q_e the adsorption capacities at time t (mg of adsorbat·g^{-1} of adsorbent) and at equilibrium (mg of adsorbat·g^{-1} of adsorbent), respectively. L'intégration de l'équation (Equation (4)) donne:

$$\ln\left(q_e - q_t\right) = \ln q_e k_1 t \tag{5}$$

The value of k_1 is obtained from the slope of the linear plot of $\ln\left(q_e - q_t\right) = f\left(t\right)$.

2) Pseudo-second order model

An expression also very often used is that of pseudo-second order. It is represented by the formula (Equation (6)) [10]:

$$\frac{\mathrm{d}q_t}{\mathrm{d}t} = k_2\left(q_e - q_t\right)^2 \tag{6}$$

With k_2 the rate constant for second order kinetics ($\mathrm{g{\cdot}mg^{-1}{\cdot}min^{-1}}$), q_t and q_e the adsorption capacities at time t (mg of adsorbate·g^{-1} of adsorbent) and at equilibrium (mg of adsorbate·g^{-1} of adsorbent), respectively. The integration of equation (Equation (6)) leads to (Equation (7)):

$$\frac{t}{q_t} = \frac{t}{q_e} + \frac{1}{k_2 \cdot q_e^2} \tag{7}$$

The pseudo-second order model is verified when the plot against t gives a linear relationship, with a slope equal to $\left(\frac{1}{k_2 \cdot q_e^2}\right)$.

3. Results and Discussion

3.1. Results

3.1.1. Characterization of Clay Material

1) pH at point of zero charge ($\mathrm{pH_{PZC}}$)

The $\mathrm{pH_{PZC}}$ curves were obtained according to our experimental procedure described previously. **Figure 3** shows that the pHs of zero charge ($\mathrm{pH_{PZC}}$) are 5.5 for AB clay and 6.08 for Aga clay. Both clays have a slightly acidic $\mathrm{pH_{PZC}}$.

The curves made it possible to determine the $\mathrm{pH_{PZC}}$ of the different clays. This value is 5.5 for AB and 6.08 for Aga. At pH < $\mathrm{pH_{PZC}}$, the surface of the clay acquires positive charges. There will, therefore, be an excess of $\mathrm{H^+}$ ions which will compete with the cations of the dye to access the clay adsorption sites [11]. Electrostatic repulsion causes a decrease in the amount of dye absorption. At pH > $\mathrm{pH_{PZC}}$ values, the surface of the clay will be negatively charged facilitating an association

between the cationic dye [12]. The pH of the BM solution is 7 higher than the pH at the zero charge point of the clays, so the pH of the solution will be used for the rest of our work.

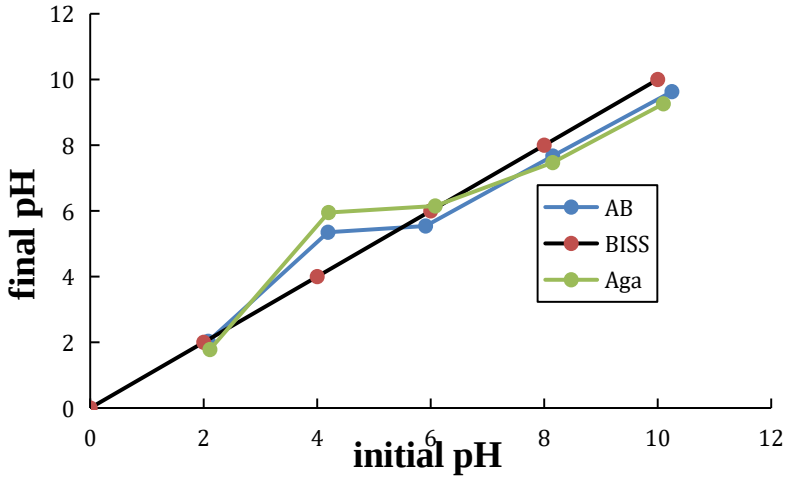

Figure 3. Determination of pH_{PZC} of AB and Aga clays.

2) Chemical analysis

The chemical analysis of AB and Aga clays was carried out by ICP-AES Plasma Emission spectrometry after chemical solution using a microwave. The chemical composition expressed as oxide is given in **Table 1**. The results show a predominance of silica (SiO_2) and alumina (Al_2O_3) in the two raw materials. Potassium, sodium and titanium oxides are also present in relatively small quantities. Calcium and manganese are found in trace amounts in clays. These high contents of SiO_2 and Al_2O_3 show that they are aluminosilicates [13]. The silica/alumina ratio (SiO_2/Al_2O_3) is 10.44 for Aga and 2.18 for AB. This ratio is high in both samples instead of 1.18 for pure kaolins [14]. These high values suggest the presence of a large amount of free silica and type 2/1 clay.

Table 1. Chemical composition of clay (% by mass of oxide).

Samples	SiO_2	Al_2O_3	Fe_2O_3	K_2O	TiO_2	Na_2O	Si_2O/Al_2O_3	Total
AB	62.40	28.60	3.20	1.30	0.90	0.80	2.18	97.20
Aga	86.92	8.32	2.81	1.01	0.74	0.19	10.44	99.99

3) X-ray diffraction

The X-ray diffractograms of the two samples AB and Aga are shown in **Figure 4**. All peaks have been assigned. The X-ray spectrum of Aga clay highlights the characteristic lines of kaolinite (12˚; 20˚; 25˚; 35˚), illite (37˚), quartz (20˚; 26˚; 45˚; 50˚) and goethite (41˚). The diffractogram of AB presents the lines of kaolinite (12˚; 25˚; 35˚), quartz (26˚; 36˚; 50˚) and illite (9˚; 19.70˚; 29.36˚) [15].

The results obtained in XRD are consistent with those of the chemical analysis.

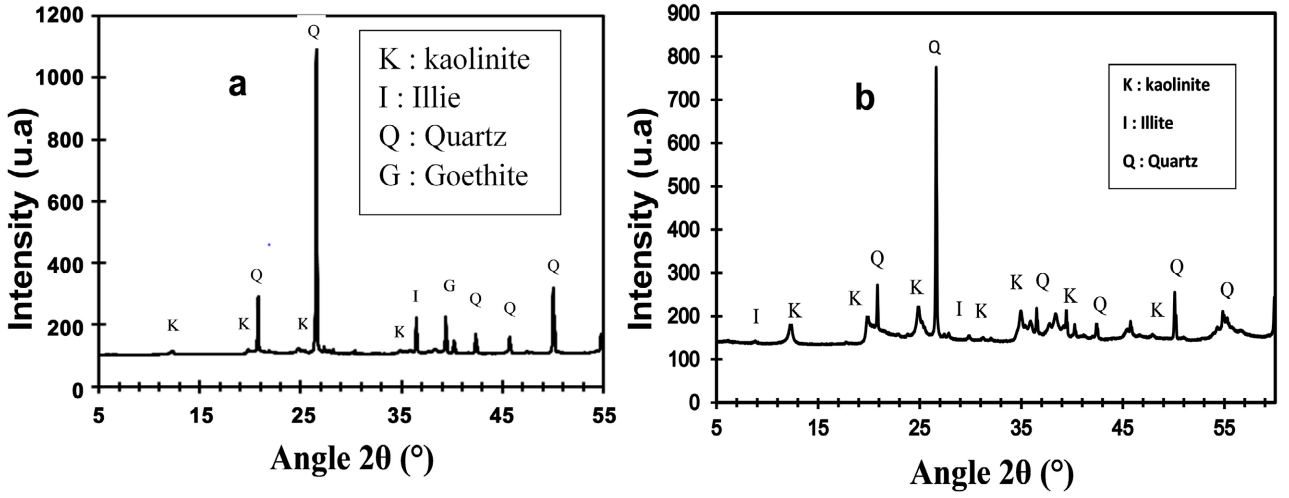

Figure 4. Diffractograms of clays: (a) Aga and (b) AB.

4) Mineralogical composition

The mineralogical composition of AB and Aga clays was estimated from the chemical analysis and the chemical composition of the mineralogical phases detected by X-ray diffraction. The results obtained are recorded in Table 2.

Table 2. Mineralogical compositions.

Samples (%)	Kaolinite	Quartz	Illite	Goethite	Total
AB	61.36	28.60	10.10	-	100.05
Aga	12.72	75.43	8.75	3.12	100.02

5) Infrared spectroscopy

The infrared spectra of Aga clay and AB clay are shown in Figure 5. In the 3000 - 4000 cm^{-1} range, the following are observed:

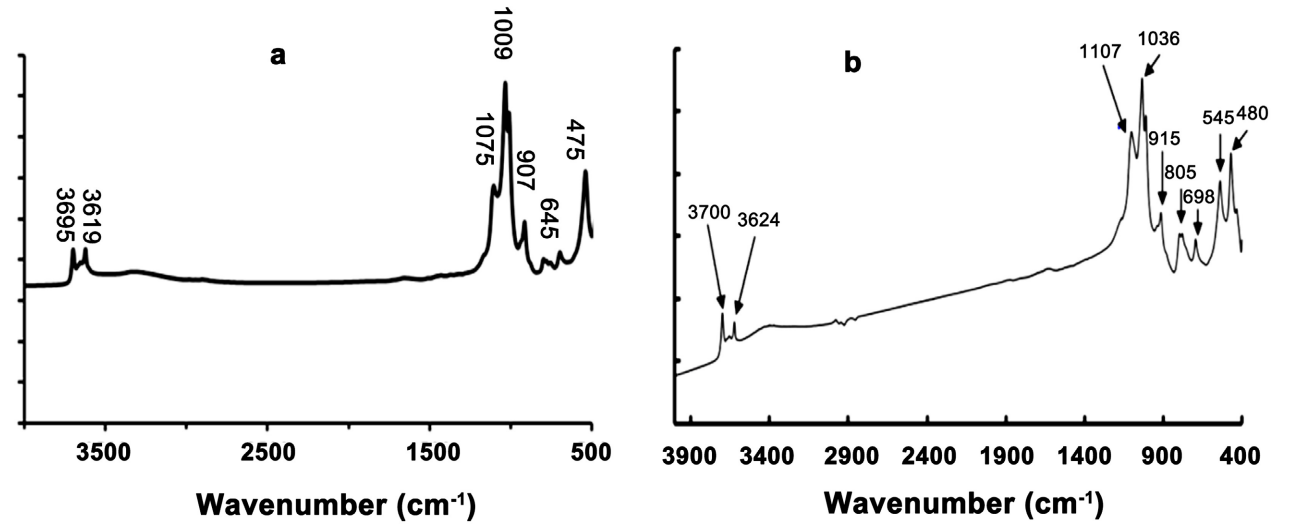

Figure 5. Infrared spectra of clays: (a) AB and (b) Aga.

For the Aga and AB samples, bands at (3700 cm^{-1} and 3624 cm^{-1}) and (3695 cm^{-1} and 3619 cm^{-1}) which are characteristic of kaolinite due to stretching vibrations of the hydroxyl groups [16] [17]. The band at 3700 cm^{-1} in particular corresponds to the vibrations of the external hydroxyls of the kaolinite and that at 3624 cm^{-1} to the vibrations of the internal hydroxyls located between the layers. This same band at 3624 cm^{-1} is also characteristic of the stretching vibration of the OH bond of the mainly Al-OH-Al network of illite. These bands have been the subject of several studies. The band at 3695 cm^{-1} is attributed to the hydroxyls at the edges of the sheet. The one located at 3619 cm^{-1} is linked to the internal hydroxyls.

In the range 400 - 1800 cm^{-1}:

For Aga clay:

- The bands observed at 805, 1107, 1036 cm^{-1} are characteristic of kaolinite. At 1107 cm^{-1} we have vibrations of the Si-O bond (symmetric), while at 1036 cm^{-1} it is vibrations of the Si-O-Si bond (antisymmetric) [18]-[21].
- As for the band at 915 cm^{-1} which can be attributed to the Al-OH deformation vibrations of kaolinite and illite.
- a band at 698 cm^{-1} corresponds to the Si-O-Si elongation vibration of quartz.
- The bands of 545 and 480 cm^{-1} can also be attributed to kaolinite. That at 545 cm^{-1} corresponds to the deformation vibration of the Si-O-Al bond of kaolinite and 480 cm^{-1} corresponds to the deformation vibration of the Si-O-Si bond of kaolinite.

For AB clay:

- The bands observed at 1009, 1075 cm^{-1} are characteristic of kaolinite. At 1009 cm^{-1} we have vibrations of the Si-O bond (symmetric), while at 1075 cm^{-1} it is vibrations of the Si-O-Si bond (antisymmetric) [18] [21] [22];
- As for the band at 907 cm^{-1} which can be attributed to the Al-OH deformation vibrations of kaolinite and illite;
- a band at 645 cm^{-1} corresponds to the Si-O-Si elongation vibration of quartz,
- The band at 475 cm^{-1} cans also be attributed to kaolinite. It corresponds to the deformation vibration of the Si-O-Si bond of kaolinite.

3.1.2. Degradation of Methylene Blue by The Photo-Fenton Process

1) Effect of hydrogen peroxide

All experiments were carried out under daylight irradiation. To study the action of hydrogen peroxide on the degradation of Methylene Blue, it is important to determine the optimal quantity of H_2O_2 necessary for maximum degradation of the dye. To do this, 20 mg of ferrous iron was fixed, then the quantity of H_2O_2 (30%) was varied in steps of 0.1 mL in an interval of 0.1 mL to 0.5 mL, for a solution of BM concentration 50 $mg{\cdot}L^{-1}$. **Figure 6** shows the different yields for each quantity of H_2O_2 after 2 hours.

The degradation rate of MB reached more than 90% after 120 minutes of reaction. The optimal quantity of H_2O_2 retained for the degradation of MB is 0.1 mL because it makes it possible to obtain a satisfactory rate for a small quantity of reagent.

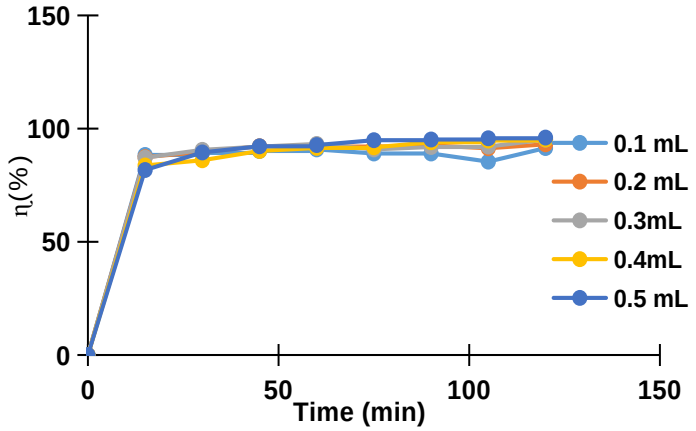

Figure 6. Effect of hydrogen peroxide.

2) Kinetics of MB degradation by hydrogen peroxide

The pseudo-first order and pseudo-second order kinetic laws were investigated in this study.

➢ **Pseudo First Order Kinetics**

The plot of $\ln(q_e - q_t)$ as a function of time t for the degradation of MB by hydrogen peroxide gives linear shapes (Figure 7).

The values of k_1 were calculated from the slopes of these lines, and $q_{e\text{cal}}$ from the ordinate at the origin. The kinetic constant of the pseudo-first-order degradation reaction k_1, the quantity of MB adsorbed at equilibrium q_e, and the correlation coefficient R_1^2 are shown in Table 3. The results in Table 3 show that the correlation coefficients obtained are 0.4308 for 0.2 mL and 0.1227 for the quantity of 0.5 mL. Despite the high correlation coefficient values, the experimental q_e do not agree with the q_e calculated from linearized forms of pseudo-first order kinetics. Therefore, the pseudo-first order kinetic model is not well suited to describe the degradation of MB by hydrogen peroxide.

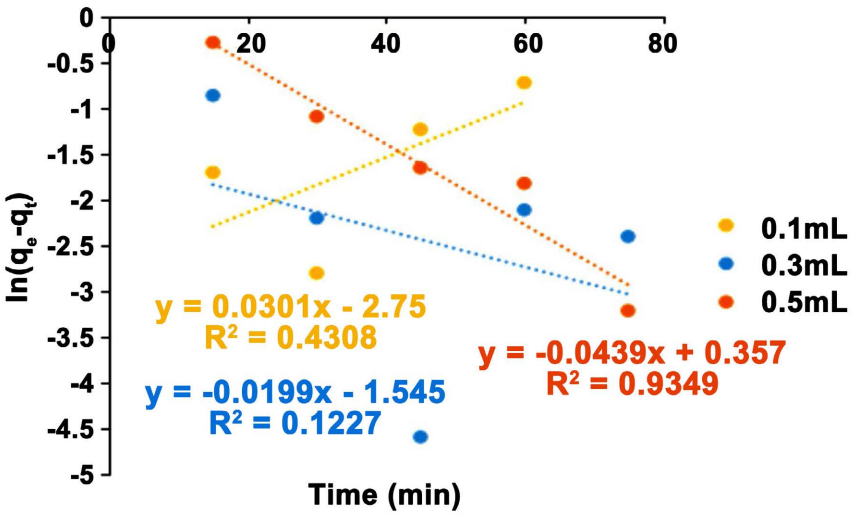

Figure 7. Pseudo first order kinetics for MB degradation by oxygen.

Table 3. Pseudo-first order kinetic constants for MB degradation by hydrogen peroxide.

	Quantity (mL)	$q_{e,exp}$ (mg/g)	$q_{e,cal}$ (mg/g)	k_1 (min^{-1})	R_1^2
H_2O_2	0.1	12.36	0.98	0.00448	0.4306
	0.3	6.27	1.04	0.024	0.1227
	0.5	5.08	1.43	0.0439	0.9349

➢ **Pseudo-Second Order Kinetics**

The plot of versus time t for the degradation of MB by hydrogen peroxide gives the linear forms (Figure 8). The values of k_2 and q_e can be determined from the slopes and y-intercepts of these lines.

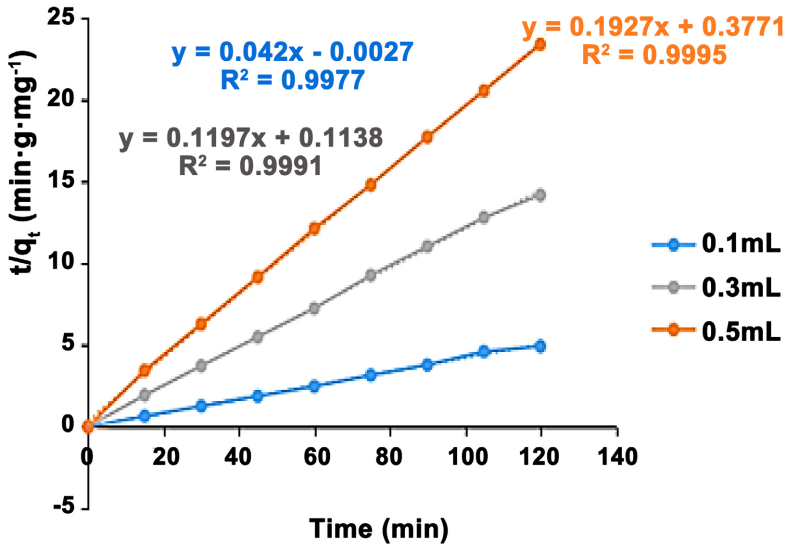

Figure 8. Pseudo-second order kinetics for MB degradation by hydrogen peroxide.

The pseudo-second order degradation kinetic constant k_2, the quantity of MB adsorbed at equilibrium q_e, and the correlation coefficient R_2^2 are indicated in Table 4. From these results, we note that the correlation coefficients R_2^2 are greater than the R_1^2 coefficients for all quantities of hydrogen peroxide. Furthermore, the experimental q_e values are much closer to the q_e values calculated from the linear forms of the pseudo-second order kinetics for all quantities of hydrogen peroxide. From these results, it appears that the pseudo-second order kinetic model gives a better description of the kinetics of the MB degradation reaction with hydrogen peroxide, unlike the pseudo-first order kinetic model.

Table 4. Pseudo-second order kinetic constants for MB degradation by oxygen.

	Quantity (mL)	$q_{e,exp}$ (mg/g)	$q_{e,cal}$ (mg/g)	k_2 (min^{-1})	R_2^2
H_2O_2	0.1	12.36	12.40	0.14	0.9977
	0.3	6.27	6.41	0.07	0.9991
	0.5	5.08	5.19	0.1	0.9995

3) Effect of iron (Fe^{2+})

Ferrous iron plays an important role in the efficiency of the photo-Fenton process. For the determination of its optimal value for the degradation of methylene blue is essential. For this, the optimal quantity of H_2O_2 is set at 0.1 ml and the mass of Iron is varied from 5 to 25 mg in steps of 5 mg. The results are presented in Figure 9.

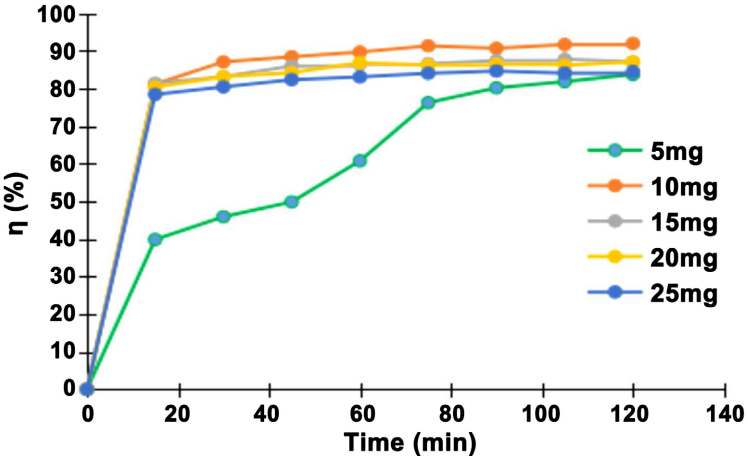

Figure 9. Effect of ferrous iron.

The degradation rate of Methylene Blue changes rapidly when the quantity of iron varies from 0 to 15 minutes. After 15 minutes, the yield is constant with an elimination rate of more than 90% for the different quantities. For the quantity of 10 mg, the elimination rate is BM is 92% after 120 minutes. This yield being the best, the quantity of iron of 10 mg will be retained as the optimal value for the rest of the work.

4) Kinetics of MB degradation by ferrous iron

The pseudo-first order and pseudo-second order kinetic laws were used in this study.

➢ **Pseudo-Second Order Kinetics**

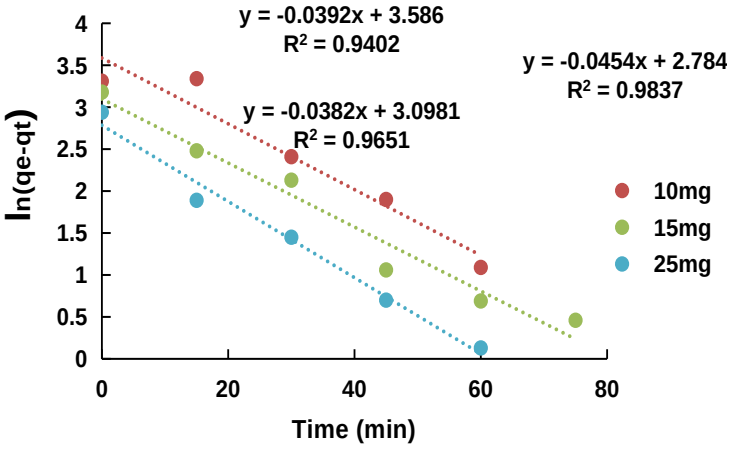

Figure 10. Pseudo-first order kinetics for BM degradation by iron.

The plot of $\ln(q_e - q_t)$ versus time t for the degradation of MB by iron gives linear shapes (Figure 10).

The values of k_1 were calculated from the slopes of these lines, and $q_{e,cal}$ from the ordinate at the origin. The pseudo-first order degradation kinetic constant k_1, the quantity of MB adsorbed at equilibrium q_e, and the correlation coefficient R_1^2 are shown in Table 5.

Table 5. Pseudo-first order kinetic constants for the degradation of MB iron.

	Quantity (mg)	$q_{e,exp}$ (mg/g)	$q_{e,cal}$ (mg/g)	k_1 (min^{-1})	R_1^2
Iron	10	268.18	36.09	0.0392	0.9402
	15	172.89	22.15	0.0382	0.9651
	25	99.7	16.18	0.0454	0.9837

The results in Table 5 show that, the correlation coefficients obtained are 0.9402 for 10 mg; 0.9651 for 15 mg and 0.9837 for 25 mg. Despite the high correlation coefficient values, the experimental q_e do not agree with the q_e calculated from linearized forms of pseudo-first order kinetics. Therefore, the pseudo-first-order kinetic model is not well suited to describe the degradation of MB by iron.

➢ **Pseudo-Second Order Kinetics**

The plot of versus time t for the degradation of MB by ferrous iron gives the linear shapes (Figure 11). The values of k_2 and q_e can be determined from the slopes and y-intercepts of these lines. The kinetic constant of the pseudo-second order adsorption reaction k_2, the quantity of phenol adsorbed at equilibrium q_e and the correlation coefficient R_2^2 are shown in Table 6.

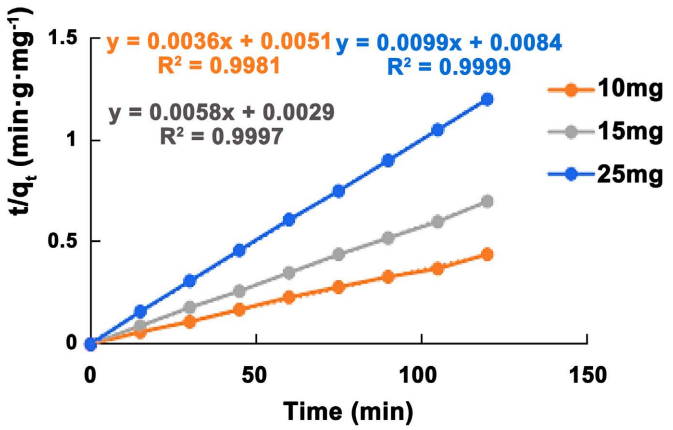

Figure 11. Pseudo-second order kinetics for MB degradation by iron.

Table 6. Pseudo-second order kinetic constants for MB degradation by iron.

	Quantity (mg)	$q_{e,exp}$ (mg/g)	$q_{e,cal}$ (mg/g)	k_2 (min^{-1})	R_2^2
Iron	10	268.18	277.78	0.0025	0.9981
	15	172.89	172.41	0.0116	0.9997
	25	99.70	101.01	0.0116	0.9999

From these results, we notice that the R_2^2 correlation coefficients are greater than the R_1^2 coefficients for all pseudo-first order iron quantities. Furthermore, the experimental q_e values are much closer to the q_e values calculated from the linear forms of the pseudo-second order kinetics for all quantities of iron. From these results, it appears that the pseudo-second order kinetic model gives a better description of the kinetics of MB degradation by iron, unlike the pseudo-first order kinetic model.

5) Influence of clay

For the study of the influence of clay on the removal of BM the optimal values of peroxide and iron were used in the photo-Fenton process. Then the masses of the AB and Aga clays were varied from 0.05 g to 0.2 g in steps of 0.05 g over a period of 2 hours. The results obtained are presented in Figure 12. For all quantities of clay used, the removal rate is high ($\eta > 90\%$). Among the clay masses used, for masses of 0.05 to 0.15 g, a rapid increase in the elimination rate is observed, from 15 to 40 minutes the yield is constant at 98%. Beyond 40 minutes a decrease in the elimination rate of methylene blue is observed. Thus, in the case of our study, the optimal mass of clay necessary for the effective elimination of methylene blue (50 mg/L) is 0.1 g.

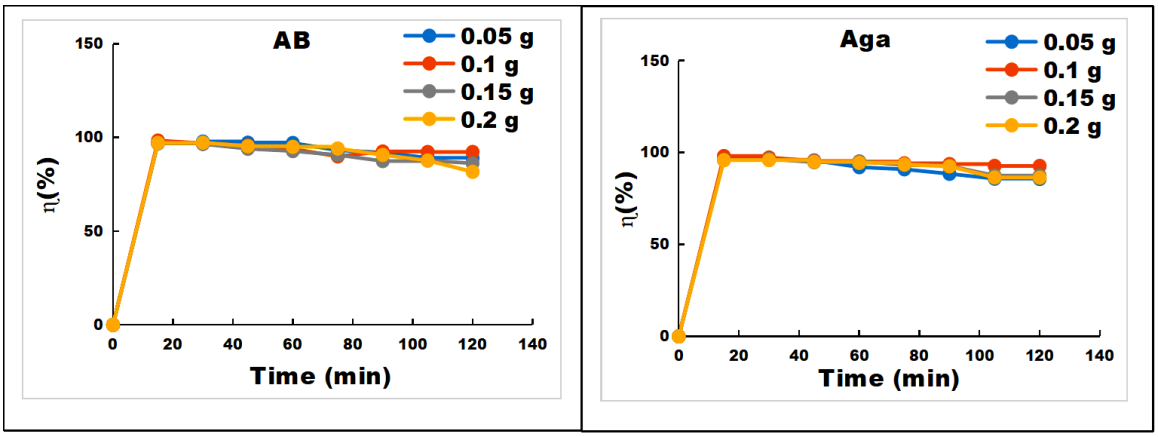

Figure 12. Influence of the quantity (AB and Aga) in the elimination of Methylene Blue by photo-Fenton process.

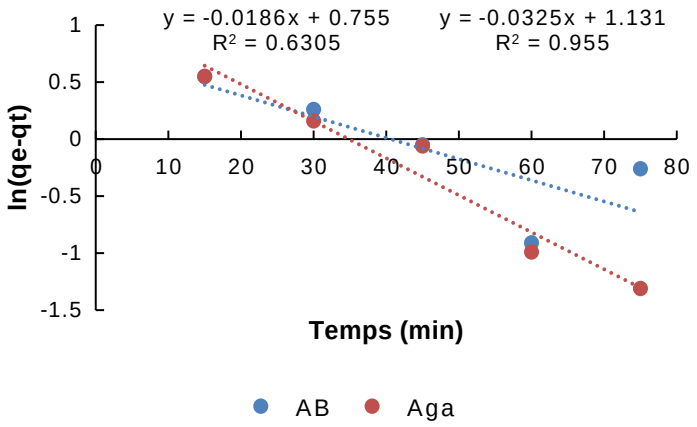

Figure 13. Pseudo first order kinetics for MB degradation with the influence of clay.

6) Kinetics of MB degradation by the influence of clay

During this study, pseudo-first order and pseudo-second kinetic laws were used. The plot of $\ln(q_e - q_t)$ as a function of time t for the degradation of MB with the influence of clay gives linear shapes (Figure 13). The values of k_1 were calculated from the slopes of these lines, and $q_{e,cal}$ from the ordinate at the origin.

➢ **Pseudo-Second Order Kinetics**

The pseudo-first order degradation kinetic constant k_1, the quantity of MB adsorbed at equilibrium q_e, and the correlation coefficient R_1^2 are shown in Table 7.

Table 7. Pseudo-first order kinetic constants for MB degradation with the influence of clay

	Quantité (g)	$q_{e,exp}$ (mg/g)	$q_{e,cal}$ (mg/g)	k_1 (min^{-1})	R_1^2
AB	0.1	27.45	2.13	0.0186	0.6305
Aga	0.1	27.92	3.1	0.0325	0.955

The results in Table 7 show that the correlation coefficients obtained are 0.6305 for 0.1 g of AB and greater than 0.95 for the quantity of 0.1 g of Aga clay. Despite the high correlation coefficient values, the experimental q_e does not agree with the q_e calculated from linearized forms of pseudo-first order kinetics. Therefore, the pseudo-first order kinetic model is not well suited to describe the degradation of MB with the influence of clay.

➢ **Cinetique of pseudo-second order**

The plot of versus time t for the degradation of MB with the influence of clay gives linear shapes (Figure 14).

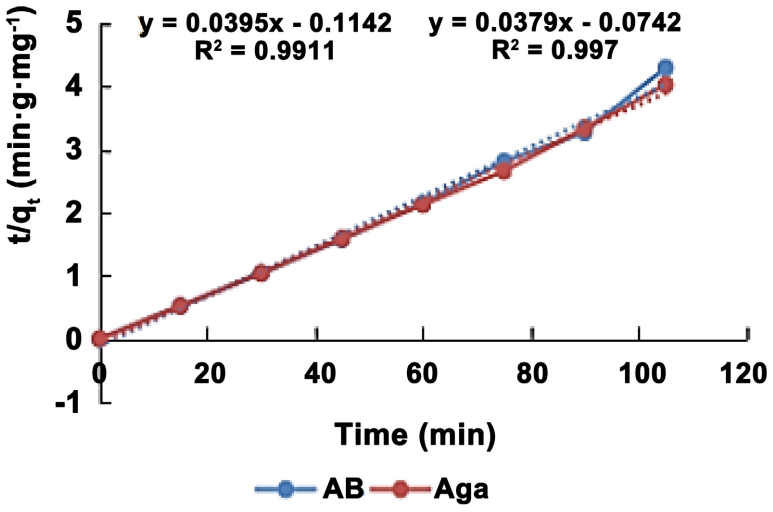

Figure 14. Pseudo-second order kinetics for MB degradation with the influence of clay.

The kinetic constant of the pseudo-second order adsorption reaction k_2, the quantity of phenol adsorbed at equilibrium q_e, and the correlation coefficient R_2^2 are shown in Table 8.

Table 8. Pseudo-second order kinetic constants for MB degradation with the influence of clay.

	Quantity (g)	$q_{e,exp}$ (mg/g)	$q_{e,cal}$ (mg/g)	k_2 (min^{-1})	R_2^2
AB	0.10	27.45	25.32	−0.014	0.9911
Aga	0.10	27.92	26.36	−0.019	0.997

The best model established for the study of degradation kinetics is chosen according to the correlation factor. The higher this factor is and closer to 1, the more favorable the model is for studying the degradation process [23]. In **Table 7**, we notice that the R_2^2 correlation coefficients are greater than the R_1^2 coefficients for all quantities of clays. In addition, the experimental q_e values are much closer to the q_e values calculated from the linear forms of the pseudo-second order kinetics for all quantities of hydrogen peroxide. From these results, it appears that the pseudo-second order kinetic model gives a better description of the reaction kinetics of MB degradation with the influence of clay, unlike the pseudo-first order kinetic model.

3.2. Discussion

The degradation of Methylene Blue by the photo-Fenton process was carried out in the presence of natural light. First, the volume of peroxide required for maximum dye removal was determined by setting the iron at 20 mg and varying the peroxide from 0.1 mL to 0.5 mL. Then, the optimal amount of iron was determined by setting the optimal volume of peroxide determined previously and varying the amounts of iron from 5 mg to 25 mg. Indeed, due to its low oxidizing power (1.8 V/ENH compared to 2.8 V/ENH for the hydroxyl radical), hydrogen peroxide is not capable of degrading MB alone [24]. On the other hand, when associated with ferric ions, it produces hydroxyl radicals which eliminate the dyes. Nicol showed that the use of 1 to 2 M hydrogen peroxide would improve the efficiency of dye processing, but only when H_2O_2 was coupled to ferric ions at 0.2 M [25]. The amount of 0.1 mL of hydrogen peroxide allowed the elimination of 90% of the dye, so it was chosen as the optimal value. Wei *et al.* showed that an excess amount of H_2O_2 could decrease the degradation rate due to competitive reactions between H_2O_2 and free radicals, which could reduce the efficiency of the process [26]. The optimal amount of ferrous iron for dye degradation is 10 mg for a yield of 92%. Beyond this value, the yield decreases. This observation could be explained by the formation of aggregates which would reduce the number of active sites [27] [28]. The decolorization rate of Methylene Blue when adding 0.1 g of AB and Aga clays made it possible to obtain a removal of 98.43% for AB and 98.13% for Aga. This could be explained by two phenomena that occur simultaneously during processing: the adsorption of the dye by the clay and the photo-Fenton process. Indeed, the mineralogical composition of the clays showed that these clays contain a significant proportion of clay minerals. These minerals have a strong adsorbent power due to the small size of their particles which gives them a

large specific surface area. Indeed, Karim *et al.* in their study, showed that the adsorption process on raw MB clay is very rapid during the first 10 minutes of treatment and evolves slowly then stabilizes after the 40th minute [29]. Their results show that 95% of the adsorbed quantity was reached during the first ten minutes. Beyond this quantity of clay, we observe a reduction in the rate of elimination of the pollutant. This may be due to the difficulty of MB molecules in reaching the absorbing sites [30]. When the quantity of clay increases, we witness the phenomenon of agglomeration of clay particles. The solution becomes cloudier, which leads to a decrease in the effectiveness of the catalyst observed by the drop in the amount of light in the liquid, consequently the number of hydroxyl radicals responsible for degradation is reduced. Furthermore Badis and Manaa showed it for the elimination of two pollutants by photo-induction and the elimination of pharmaceutical compounds by photo-Fenton [2] [31]. This same observation was made by Saoudi and Hamouma [32]. According to them, this behavior can be explained:

- As long as the amount of adsorbent added to the dye solution is small, the dye cations can easily access the adsorption sites. The addition of adsorbent makes it possible to increase the number of adsorption sites, but the cations of the dye have more difficulty approaching these sites because of the congestion;
- A large quantity of adsorbent can create agglomerations of particles, resulting in a reduction in the total adsorption surface and, consequently, a reduction in the quantity of adsorbate per unit mass of adsorbent.

It is also noted that the amount of adsorption is slightly higher for AB clay than Aga clay. The comparison of the two clays allows us to conclude that AB clay has greater adsorbent power than Aga clay. This is reflected in the characteristics of the clays contained in **Table 2**. Indeed, AB clay is richer in clay minerals with a rate of 70.06% unlike Aga clay which has 21.44% clay minerals. In addition, goethite, which represents 3.12% of Aga clay and which is absent in AB clay, is a mineral which also has adsorption properties. It contributes to the high adsorption capacity of Aga clay.

4. Conclusions

This work aims to promote local materials with a view to using them for wastewater treatment. It is in this context that AB and Aga clays were characterized. The characterization results showed that AB clay is mainly composed of kaolinite (61.31%), quartz (28.9%) and illite (11.26%). As for Aga clay, it is composed of kaolinite (12.72%), quartz (77.13%), illite (8.75%) and a small proportion of goethite (3.12%). From these characterizations, it appears that AB clay with a significant proportion of kaolinite can be used for the adsorption of methylene blue and the proportion of goethite in Aga clay would favor the adsorption phenomenon. Subsequently, the optimal quantities of the reagents of the Fenton process, namely hydrogen peroxide (0.1 mL) and ferrous iron (10 mg) were determined under daylight irradiation. Finally, we carried out an experimental study

of the influence of different clays on the degradation of MB by the photo-Fenton process. The results obtained during our study were able to highlight the following considerations:

- The photo-Fenton process eliminates 92% of BM;
- The combination of adsorption and photo-Fenton process made it possible to eliminate more than 98% of the pollutant for both types of clay.

It should also be noted that the degradation of methylene blue follows pseudo-second order kinetics. In summary, we conclude that the photo-Fenton process is effective for the elimination of the dye. However, it is the addition of clay which allows it to achieve a suitable elimination efficiency for industries because the combination of these two processes made it possible to obtain an efficiency of 98.43% for AB and 98.13% for Aga. This study can continue, by testing other types of materials in order to obtain a material that can completely eliminate the pollutant and study the adsorption isotherms.

Conflicts of Interest

The authors declare no conflicts of interest regarding the publication of this paper.

References

[1] Bhuiyan, M.A.R., Islam, A., Ali, A. and Islam, M.N. (2017) Color and Chemical Constitution of Natural Dye Henna (*Lawsonia inermis* L) and Its Application in the Coloration of Textiles. *Journal of Cleaner Production*, **167**, 14-22. https://doi.org/10.1016/j.jclepro.2017.08.142

[2] Manaa, Z. (2015) Élimination des composes pharmaceutiques par photo-Fenton heterogene (goethite et argile synthétique): Etude cinétique et transfert des espèces organiques à l'interface minéral solution. Master's Thesis, Université Ferhat Abbas Sétif. http://dspace.univ-setif.dz:8888/jspui/bitstream/123456789/1698/1/elimination%20de%20SMX%20par%20photofenton.pdf

[3] Ali, I., Asim, M. and Khan, T.A. (2012) Low Cost Adsorbents for the Removal of Organic Pollutants from Wastewater. *Journal of Environmental Management*, **113**, 170-183. https://doi.org/10.1016/j.jenvman.2012.08.028

[4] De Gisi, S., Lofrano, G., Grassi, M. and Notarnicola, M. (2016) Characteristics and Adsorption Capacities of Low-Cost Sorbents for Wastewater Treatment: A Review. *Sustainable Materials and Technologies*, **9**, 10-40. https://doi.org/10.1016/j.susmat.2016.06.002

[5] Barka, N., Assabbane, A., Nounah, A., Albourine, A. and Ait-Ichou, Y. (2008) Degradation Photo-catalytique de deux colorants separés et en mélange Binaire Par TiO_2-Supporte. *Sciences & Technologie A*, No. 27, 9-16.

[6] Lopez-Ramon, M.V., Stoeckli, F., Moreno-Castilla, C. and Carrasco-Marin, F. (1999) On the Characterization of Acidic and Basic Surface Sites on Carbons by Various Techniques. *Carbon*, **37**, 1215-1221. https://doi.org/10.1016/s0008-6223(98)00317-0

[7] N'guessan, J.K. (2010) Etude expérimentale et modélisation d'un procédé séquentiel AD-OX d'élimination de polluants organiques. Doctorat Thesis, Institut National Polytechnique de Toulouse.

[8] Voïnovitch, I.A. (1988) Analyse des sols, roches et ciments: Méthodes choisies. Dunod.

[9] Lagergren, S. (1898) Zur theorie der sogenanten adsorption geloster stoffe, Kungliga Svenska Vetenskaps akademiens. *Handlingar*, **24**, 1-39.

[10] Messeaouda, S. (2015) Etude de la capacité de rétention et d'élimination des cations métalliques par des adsorbants naturels. https://www.theses-algerie.com

[11] Elmoubarki, R., Mahjoubi, F.Z., Tounsadi, H., Moustadraf, J., Abdennouri, M., Zouhri, A., *et al.* (2015) Adsorption of Textile Dyes on Raw and Decanted Moroccan Clays: Kinetics, Equilibrium and Thermodynamics. *Water Resources and Industry*, **9**, 16-29. https://doi.org/10.1016/j.wri.2014.11.001

[12] Miyah, Y., Lahrichi, A., Idrissi, M., Khalil, A. and Zerrouq, F. (2018) Adsorption of Methylene Blue Dye from Aqueous Solutions onto Walnut Shells Powder: Equilibrium and Kinetic Studies. *Surfaces and Interfaces*, **11**, 74-81. https://doi.org/10.1016/j.surfin.2018.03.006

[13] Nirmala, G. and Viruthagiri, G. (2015) A View of Microstructure with Technological Behavior of Waste Incorporated Ceramic Bricks. *Spectrochimica Acta Part A*: *Molecular and Biomolecular Spectroscopy*, **135**, 76-80. https://doi.org/10.1016/j.saa.2014.06.150

[14] Amon, L.N., Konan, L.K., Goure-Doubi, H., Andji, J.Y.Y., Coulibaly, J.K. and Oyetola, S. (2017) Physico-Chemical and Structural Properties of Clay-Based Ceramic Filters from Côte d'Ivoire. *Journal de la Société Ouest-Africaine de Chimie*, **44**, 70-77.

[15] Méité, N., Marie-Sandrine Kouakou, L.P., Kouamé, A.N., Kouassi, S.S., Silva e Silva, C., Sidibe Sandé, S.L., *et al.* (2024) Physical and Chemical Properties of Cassava Starch Biopolymer Reinforced with Coconut Fiber and/or Metakaolin. *Journal of the Indian Chemical Society*, **101**, Article 101185. https://doi.org/10.1016/j.jics.2024.101185

[16] Madejová, J. (2003) FTIR Techniques in Clay Mineral Studies. *Vibrational Spectroscopy*, **31**, 1-10. https://doi.org/10.1016/s0924-2031(02)00065-6

[17] Konan, K.L., Soro, J., Andji, J.Y.Y., Oyetola, S. and Kra, G. (2010) Etude comparative de la déshy-droxylation/amorphisation dans deux kaolins de cristallinité différente. *Journal de la Société Ouest-Africaine de Chimie*, **30**, 29-39.

[18] Kouame, A.N., Ouedraogo, M., Manouan, W.M.R., Kouakou, L.P.M., Meite, N., Doubi, B.I.H.G., *et al.* (2023) Influence of the Size of Soursop Seed Granules on the Mechanical and Water Properties of Compressed Earth Bricks. *International Journal of Chemistry and Materials Research*, **11**, 23-31. https://doi.org/10.18488/64.v11i2.3581

[19] Méité, N. (2019) Physico-Chemical Behavior of Glycerol-Coated Cassava Starch Gels Incorporating Kaolin and Metakaolin. *American Journal of Materials Science and Engineering*, **7**, 1-6.

[20] Méité, N., Konan, L.K., Tognonvi, M.T., Doubi, B.I.H.G., Gomina, M. and Oyetola, S. (2021) Properties of Hydric and Biodegradability of Cassava Starch-Based Bioplastics Reinforced with Thermally Modified Kaolin. *Carbohydrate Polymers*, **254**, Article 117322. https://doi.org/10.1016/j.carbpol.2020.117322

[21] Sanou, A., Coulibaly, S., Kouaménan, N.M., Méité, N., N'Dri, S.N. and Atsé, B.C. (2021) Evaluation of Potential Risks of Farmed Fish Consumption on Human Health. *Sciences des Structures et de la Matière*, **4**, 17-30. http://publication.lecames.org/index.php/mat/article/view/2295

[22] Sanou, I., Ouedraogo, M., Bamogo, H., Meité, N., Seynou, M., Aubert, J., *et al.* (2024) Microstructural, Physical, and Mechanical Characteristics of Adobes Amended with Cement-Metakaolin Mixtures. *Emergent Materials*, **7**, 1203-1217. https://doi.org/10.1007/s42247-024-00638-9

[23] Ho, Y. (2003) Removal of Copper Ions from Aqueous Solution by Tree Fern. *Water Research*, **37**, 2323-2330. https://doi.org/10.1016/s0043-1354(03)00002-2

[24] Guittonneau, S., De Laat, J., Dore, M., Duguet, J.P. and Honnel, C. (2005) Etude de la dégradation de quelques composés organochlorés volatils par photolyse du peroxyde d'hydrogène en milieux aqueux. *Revue des sciences de l'eau*, **1**, 35-54. https://doi.org/10.7202/705002ar

[25] Nicol, M.J. (2020) The Role and Use of Hydrogen Peroxide as an Oxidant in the Leaching of Minerals. 1. Acid Solutions. *Hydrometallurgy*, **193**, Article 105328. https://doi.org/10.1016/j.hydromet.2020.105328

[26] Wei, X., Wu, H., He, G. and Guan, Y. (2017) Efficient Degradation of Phenol Using Iron-Montmorillonite as a Fenton Catalyst: Importance of Visible Light Irradiation and Intermediates. *Journal of Hazardous Materials*, **321**, 408-416. https://doi.org/10.1016/j.jhazmat.2016.09.031

[27] Zhao, T., Xu, S. and Hao, F. (2023) Differential Adsorption of Clay Minerals: Implications for Organic Matter Enrichment. *Earth-Science Reviews*, **246**, Article 104598. https://doi.org/10.1016/j.earscirev.2023.104598

[28] Omwoyo, F.O. and Otieno, G. (2024) Optimization of Methylene Blue Dye Adsorption onto Coconut Husk Cellulose Using Response Surface Methodology: Adsorption Kinetics, Isotherms and Reusability Studies. *Journal of Materials Science and Chemical Engineering*, **12**, 1-18. https://doi.org/10.4236/msce.2024.122001

[29] Karim, A.B., Mounir, B., Hachkar, M., Bakasse, M. and Yaacoubi, A. (2010) Élimination du colorant basique "Bleu de Méthylène" en solution aqueuse par l'argile de Safi. *Revue des sciences de l'eau*, **23**, 375-388. https://doi.org/10.7202/045099ar

[30] Pohan, L.A.G., Kambiré, O., Nasir, M. and Ouattara, L. (2020) Photocatalytic and Antimicrobial Properties of [$AgTiO_2$]: [Clay] Nanocomposite Prepared with Clay Different Ratios. *Modern Research in Catalysis*, **9**, 47-61. https://doi.org/10.4236/mrc.2020.94004

[31] Badis, K. (2018) Elimination de deux polluants organiques par photo-induction en phase homogène et hétérogène et par adsorption sur des supports inorganiques locaux. Thèse de doctorat, Université Frères Mentouri-Constantine 1.

[32] Saoudi, S. and Hamouma, O. (2013) Adsorption d'un colorant basique bleu de méthylène sur une argile acidifiée. Mémoire de Master, Université Abderrahmane-Mira de Béjaïa.